DISCUSSION

As shown in Figure 3, normal human osteoblasts (NHOst) in contact with microspheres showed different levels of calcium deposition only after a 1-week culture, suggesting composition of the microspheres affects NHOst differentiation level. The differentiation was suppressed by the contact with PS, PE, and alumina microspheres, while HA microspheres showed the potential to enhance the differentiation. It has been reported that GJIC plays an important role in not only the homeostasis of cells but also their differentiation.[19–22] In addition, GJIC is affected by the microsphere's composition, as has been reported using a fibroblast cell line.[18] Therefore, the results shown in Figures 1 and 2 suggest that the enhanced differentiation of NHOst relates to GJIC enhancement on a 1-day culture in contact with HA microspheres, especially the precoated microspheres. In addition, on coculture with other microspheres, GJIC was slightly suppressed at 1 day, although no significant difference compared to control NHOst was observed. We have already studied effects of the microspheres on NHOst differentiation, and enhancement of calcium deposition by coculture with the hydroxy apatite microspheres was observed. Figure 3 suggests a relationship between the calcium deposition and GJIC on day 1. This also indicates that GJIC of the NHOst, in contact with materials in the microsphere form, in the early stage may be one factor affecting their differentiation.

It has been reported that GJIC of cells derived from human osteoblasts is mainly composed of connexin 43 and 45.[22,26,27] In this study, it is also indicated that GJIC of NHOst is composed of connexin 43 and 45 (Fig. 4). Therefore, it is possible that changes in the level of their GJIC is ascribed to the change in mRNA expression level of connexin 43 and 45 and their expression ratio. From Figures 5 and 6, mRNA of connexin 43 was expressed only in normal NHOst and those cultured with PE microspheres, while it was slightly expressed in NHOst cocultured with HA. On the other hand, mRNA of connexin 45 was expressed in NHOst in all conditions, except those cocultured with alumina microspheres. Because HA was observed to enhance GJIC of NHOst, this suggests that connexin 45 may play a role in GJIC at an early stage. This also suggests that a higher level of connexin 45 than that of connexin 43 may be important in the enhancement of GJIC. However, although the mRNA expression of neither connexin 43 nor 45 was observed in NHOst cocultured with alumina microspheres, their GJIC was similar to that of normal NHOst. Moreover, it has reported that gap junctions formed by connexin 43 are more permeable to negatively charged dyes such as lucifer yellow, calcein, and carboxyfluorescein used in this study, more than those formed by connexin 45, and an increase of connexin 43 expression and GJIC function parallel osteoblast differentiation.[22,28] These are inconsistent with our findings and indicate that not high expression, but a rapid decrease of connexin 45 mRNA is probably very important for GJIC change and differentiation of the osteoblasts. Therefore, even though connexin 45 may play an important role in the early stage of GJIC in NHOst, it is probable that another connexins or other mechanisms of GJIC play a role in the GJIC of NHOst.

Because many proteins are involved in GJIC formation,[28] other mechanisms or proteins may be important in the GJIC change induced by the contact with the microspheres. It has reported that cadherins, which are important proteins for form tight junction between cells, control connexin 43-mediated GJIC.[29,30] In addition, a microtubule network inside a cell has been reported to play an important role as guidance for delivery of connexons, which are composed of six connexin molecules, to the cell membrane to make gap junctions.[31] Usually, surface characteristics of materials affect cell attachment as well as cell morphology, suggesting signal cascades of cell attachment and cytoskelton rearrangement in the cell were influenced by the characteristics. Therefore, it is probable that a surface characteristic of the microspheres affect these molecules in NHOst, resulting in changes of GJIC activities. Further studies on changes in not only connexin molecules but also other molecules such as cadherin, actin, and microtubule in NHOst, is necessary to clarify the mechanism of GJIC. In the future, we will study the above, and find another molecules participating in the GJIC of NHOst and the mechanisms regulating the connexins in NHOst.

In conclusion, the GJIC level of NHOst changes on contact with microspheres, and is affected by the composition of the microspheres. The GJIC level in the early stage might be important in the differentiation control of NHOst and the level may be controlled partly by expression of connexin 43, connexin 45, and unclarified connexins in addition to other mechanisms regulating GJIC function. Detecting a biomaterial's effect on the GJIC of human cells may be one useful method for estimating its biocompatibility.

The authors appreciate the support of Health and Labor Sciences Research Grants for Research on Advanced Medical Technology, Research on Health Sciences focusing on Drug Innovation, and Risk Analysis Research on Food and Pharmaceuticals, Ministry of Health, Labour and Welfare.

References

1. Willert HG, Semlitsch M. Reactions of the articular capsule to wear products of artificial joint prosthesis. J Biomed Mater Res 1977;11:157–164.

2. Savio JA III, Overcamp LM, Black J. Size and shape of biomaterial wear debris. Clin Mater 1994;15:101–147.
3. Wang W, Ferguson DJP, Quinn JMW, Simpson AHRW, Athanasou NA. Osteoclasts are capable of particle phagocytosis and bone resorption. J Pathol 1997;182:92–98.
4. Goodman SB, Fornasier VL, Lee J, Kei J. The histological effects on the implantation of different sizes of polyethylene particles in the rabbit tibia. J Biomed Mater Res 1990;24:517–524.
5. Kubo T, Sawada K, Hirakawa K, Shimizu C, Takamatsu T, Hirasawa Y. Histiocyte reaction in rabbit femurs to UHMWPE, metal, and ceramic particles in different sizes. J Biomed Mater Res 1999;45:363–369.
6. Shanbhag AS, Jacobs JJ, Black J, Galante JO, Glant TT. Macrophages/particle interactions: Effect of size, composition and surface area. J Biomed Mater Res 1994;28:81–90.
7. Kim KJ, Itoh T, Tanahashi M, Kumegawa M. Activation of osteoclasts-mediated bone resorption by the supernatant from a rabbit synovial cell line in response to polyethylene particles. J Biomed Mater Res 1996;32:3–9.
8. Voronov I, Santerre JP, Hinek A, Callahan JW, Sandhu J, Boynton EL. Macrophage phagocytosis of polyethylene particles in vitro. J Biomed Mater Res 1998;39:40–51.
9. Catelas I, Huk OL, Petit A, Zukor DJ, Marchand R, Yahia L. Flow cytometric analysis of macrophage response to ceramic and polyethylene particles: Effects of size, concentration, and composition. J Biomed Mater Res 1998;41:600–607.
10. Green TR, Fisher J, Stone MH, Wroblewski BM, Ingham E. Polyethylene particles of a "critical size" are necessary for the induction of cytokines by macrophages in vitro. Biomaterials 1998;19:2297–2302.
11. Green TR, Fisher J, Matthews JB, Stone MH, Ingham E. Effect of size and dose on bone resorption activity of macrophages by in vitro clinically relevant ultra high molecular weight polyethylene particles. J Biomed Mater Res (Appl Biomater) 2000; 53:490–497.
12. Takei I, Takagi M, Santavirta S, Ida H, Hamasaki M, Ishii M, Fukushima S, Ogino T, Konttinen YT. Matrix metalloproteinases and tissue inhibitors of metalloproteinases in joint fluid of the patients with loose artificial hip joints. J Biomed Mater Res 1999;45:175–183.
13. Trindade MCD, Schurman DJ, Maloney WJ, Goodman SB, Smith RL. G-protein activity requirement for polymethylmethacrylate and titanium particle-induced fibroblast interleukin-6 and monocyte chemoattractant protein-1 release in vitro. J Biomed Mater Res 2000;51:360–368.
14. Sacomen D, Smith RL, Song Y, Fornasier V, Goodman SB. Effects of polyethylene particles on tissue surrounding knee arthroplasties in rabbits. J Biomed Mater Res (Appl Biomater) 1998;43:123–130.
15. Tsuchiya T, Hata H, Nakamura A. Studies on the tumor-promoting activity of biomaterials: Inhibition of metabolic cooperation by polyetherurethane and silicone. J Biomed Mater Res 1995;29:113–119.
16. Nakaoka R, Tsuchiya T, Kato K, Ikada Y, Nakamura A. Studies on tumor-promoting activity of polyethylene: Inhibitory activity of metabolic cooperation on polyethylene surfaces is markedly decreased by surface modification with collagen but not with RGDS peptide. J Biomed Mater Res 1997;35:391–397.
17. Nakaoka R, Tsuchiya T, Nakamura A. The inhibitory mechanism of gap junctional intercellular communication induced by polyethylene and the restorative effects by surface modification with various proteins. J Biomed Mater Res 2001;57:567–574.
18. Nakaoka R, Sakaguchi K, Tsuchiya T, Nakamura A. Studies on in vitro evaluation for the biocompatibility of various biomaterials: Inhibitory activity of various kinds of polymer microspheres on metabolic cooperation. J Biomed Mater Res 2001; 57:279–284.
19. Mensil M, Krutovskikh V, Omori Y, Yamasaki H. Role of blocked gap junctional communication in non-genotoxic carcinogenesis. Toxicol Lett 1995;82/83:701–706.
20. Yamasaki H. Role of disrupted gap junctional intercellular communication in detection and characterization of carcinogens. Mutat Res 1996;365:91–105.
21. Sawada MS, Mano H, Hanada K, Kakudo S, Kameda T, Miyazawa K, Nakamaru Y, Yuasa S, Mori Y, Kumegawa M, Hakeda Y. Down-regulation of gap junctional intercellular communication between osteoblastic MC3T3–E1 cells by basic fibroblast growth factor and a phorbol ester (12-O-tetradecanoylphorbol-13-acetate). J Bone Miner Res 1997;12:1165–1173.
22. Lecanda F, Towler DA, Ziambaras K, Cheng SL, Koval M, Steinberg TH, Civitelli R. Gap junctional communication modulates gene expression in osteoblastic cells. Mol Biol Cell 1998; 9:2249–2258.
23. Nakaoka R, Tsuchiya T. Biocompatibility of various kinds of polymer microspheres estimated from their effect on gap junctional intercellular communication of fibroblasts. Mater Trans 2002;43:3122–3127.
24. Wade MH, Trosko JE, Steindler M. A fluorescence photobleaching assay of gap junctional-mediated communication between human cells. Science 1986;232:525–528.
25. Ichikawa R, Tsuchiya T. A strategy for the suppression of tumorigenesis induced by biomaterials: Restoration of transformed phenotype of polyetherurethane-induced tumor cells by Cx43 transfection. Cytotechnology 2002;39:1–8.
26. Donahue HJ, Li Z, Zhou Z, Yellowley CE. Differentiation of human fetal osteoblastic cells and gap junctional intercellular communication. Am J Physiol Cell Physiol 2000;278:C315–C322.
27. Laing JG, Manley-Markowski RN, Koval M, Civitelli R, Steinberg TH. Connexin45 interacts with zonula occludens-1 and connexin43 in osteoblastic cells. J Biol Chem 2001;276:23051–23055.
28. Duffy SH, Delmar M, Spray DC. Formation of the gap junction nexus: Binding partners for connexins. J Pathol Paris 2002;96: 243–249.
29. Jongen WMF, Fitzgerald DJ, Asamoto M, Piccoli C, Slaga TJ, Gros D, Takeichi M, Yamasaki H. Regulation of connexin 43-mediated gap junctional intercellular communication by Ca^{2+} in mouse epidermal cells is controlled by E-cadherin. J Cell Biol 1991;114:545–555.
30. Meyer RA, Laird DW, Revel JP, Johnson RG. Inhibition of gap junction and adherens junction assembly by connexin and A-CAM antibodies. J Cell Biol 1992;119:179–189.
31. Lauf U, Giepmans BNG, Lopez P, Braconnot S, Chen SC, Falk MM. Dynamic trafficking and delivery of connexins to the plasma membrane and accretion to gap junctions in living cells. Proc Natl Acad Sci USA 2002;99:10446–10451.

Available online at www.sciencedirect.com

SCIENCE DIRECT®

European Journal of Pharmacology 508 (2005) 23–30

ELSEVIER

ejp

www.elsevier.com/locate/ejphar

Characterization of voltage-dependent gating of $P2X_2$ receptor/channel

Ken Nakazawa[a,*], Yasuo Ohno[b]

[a]*Cellular and Molecular Pharmacology Section, Division of Pharmacology, National Institute of Health Sciences, 1-18-1 Kamiyoga, Setagaya, Tokyo 158-8501, Japan*

[b]*Division of Pharmacology, National Institute of Health Sciences, 1-18-1 Kamiyoga, Setagaya, Tokyo 158-8501, Japan*

Received 9 September 2004; received in revised form 29 November 2004; accepted 6 December 2004
Available online 4 January 2005

Abstract

The role of a voltage-dependent gate of recombinant $P2X_2$ receptor/channel was investigated in *Xenopus* oocytes. When a voltage step to −110 mV was applied from a holding potential of −50 mV, a gradual increase was observed in current evoked by 30 μM ATP. Contribution of this voltage-dependent component to total ATP-evoked current was greater when the current was evoked by lower concentrations of ATP. The voltage-dependent gate closed upon depolarization, and half the gates were closed at −80 mV. On the other hand, a potential at which half the gates opened was about −30 mV or more positive, which was determined using a series of hyperpolarization steps. The results of the present study suggest that the voltage-dependent gate behavior of $P2X_2$ receptor is not due to simple activation and deactivation of a single gate, but rather due to transition from a low to a high ATP affinity state.

Keywords: P2X receptor; Voltage dependence; Gate; Kinetics; Ligand affinity

1. Introduction

Extracellular ATP is considered a neurotransmitter, and its fast neurotransmission is mediated through ion channel-forming P2X receptors (see reviews, Ralevic and Burnstock, 1998; Khakh, 2001; North, 2002). To date, at least seven subclasses of P2X receptor ($P2X_{1-7}$) have been cloned, which form homo- or heteromeric receptors that act as functional ion channels (North and Surprenant, 2000). Each subclass consists of two transmembrane domains (TM1 and TM2) and one long extracellular domain (E1) between them. Both TM1 (Jiang et al., 2001; Haines et al., 2001) and TM2 (Rassendren et al., 1997; Egan et al., 1998; Migita et al., 2001) contribute to formation of the channel pore. P2X receptor/channels are permeable to cations, but demonstrate poor cation selectivity. The channels are gated by ATP molecules, and the narrowest part of the channel pore opens when activated (Rassendren et al., 1997). The ATP-binding site for gating is partly attributable to basic amino acid residues near the outer mouth of the channel pore formed by TM1 and TM2 (Ennion et al., 2000; Jiang et al., 2000), and the possibility that aromatic residues in E1 contribute to the binding site has also been suggested (Nakazawa et al., 2002; Roberts and Evans, 2004).

In addition to ATP, other factors are known to modulate channel activity. Zn^{2+} and acidic conditions facilitate ATP-mediated gating by increasing ATP sensitivity of $P2X_2$ receptor (Clyne et al., 2002). Neurotransmitters, including dopamine, and related compounds also facilitate ATP-mediated gating (Nakazawa et al., 1997a). Membrane potential may also play a role. It has been reported that ionic current activated by ATP is enhanced by hyperpolarization in pheochromocytoma PC12 cells (Nakazawa et al., 1997b). We observed similar voltage-dependent gating of recombinant $P2X_2$ receptor/channel, which was originally cloned from PC12 cells (Brake et al., 1994), and qualitatively analyzed its properties in the present study.

2. Methods

Recordings of ionic current through recombinant $P2X_2$ receptor/channels were performed according to our previous

* Corresponding author. Tel.: +81 3 3700 9704; fax: +81 3 3707 6950.
E-mail address: nakazawa@nihs.go.jp (K. Nakazawa).

0014-2999/$ - see front matter © 2004 Elsevier B.V. All rights reserved.
doi:10.1016/j.ejphar.2004.12.005

report (Nakazawa and Ohno, 1997). Briefly, the cloned rat $P2X_2$ receptor (Brake et al., 1994) was expressed in *Xenopus* oocytes by injecting in vitro transcribed cRNA. After 4 days of incubation at 18 °C, the membrane current of the oocytes was recorded. Oocytes were bathed in ND96 solution containing (in mM) NaCl 96, KCl 2, $CaCl_2$ 1.8, $MgCl_2$ 1, HEPES 5 (pH 7.5 with NaOH). In some experiments, oocytes were bathed in solution containing 10.8 mM $BaCl_2$ instead of 1.8 mM $CaCl_2$. When achieving a low extracellular chloride concentration, 96 mM Na-acetate was added instead of 96 mM NaCl. ATP (adenosine 5′-triphosphate disodium salt; Sigma, St. Louis, MO, U.S.A.) was applied by superfusion for approximately 10 s at regular 2-min intervals. Membrane current was recorded using the standard two-electrode voltage-clamp techniques, and electrical signals were stored on a data recorder (PC204Ax; SONY, Tokyo, Japan) for off-line analysis. Curve fittings to data were made using Microsoft' Excel X.

3. Results

3.1. Voltage-dependent component of ATP-evoked current

Fig. 1A compares membrane currents in the absence and presence of 30 μM ATP in a $P2X_2$ receptor-expressing oocyte. The oocyte was held at −50 mV and stepped to −110 mV for 200 ms. In the presence of ATP, inward current at −110 mV did not instantaneously reach steady-state, but gradually increased: a biphasic increase in current was observed with a voltage-independent component ("a" in Fig. 1A) and a voltage-dependent component ("b" in Fig. 1A). When the voltage was returned to −50 mV, a gradually declining inward "tail" current was observed ("c" in Fig. 1A). The voltage-dependent component of the inward current at −110 mV was observed to follow first-order kinetics with a time constant of 40 ms (Fig. 1B).

Fig. 2A demonstrates an increased magnitude of the voltage-dependent component when activated from a less negative holding potential. The voltage-dependent component was larger when the step to −110 mV was applied from −10 mV ("a" in Fig. 2A) than when it was applied from −70 mV ("b" in Fig. 2A). This dependence of the voltage-dependent component on holding potentials is illustrated in Fig. 2B. It is worth noting that Ca^{2+}-activated currents exist in *Xenopus* oocytes (Weber, 1999; Zhang and Hamill, 2000). Since P2X receptor/channels are Ca^{2+}-permeable (Khakh, 2001), a secondarily activated Ca^{2+}-induced current might contribute to the observed voltage-dependent changes. This does not, however, appear to be the case since a similar dependence on holding potentials was observed when extracellular Ca^{2+} was replaced with 10.8 mM Ba^{2+}. Time constants for the activation of the voltage-dependent component were obtained as shown in Fig. 1B, and the mean values were plotted against holding potentials

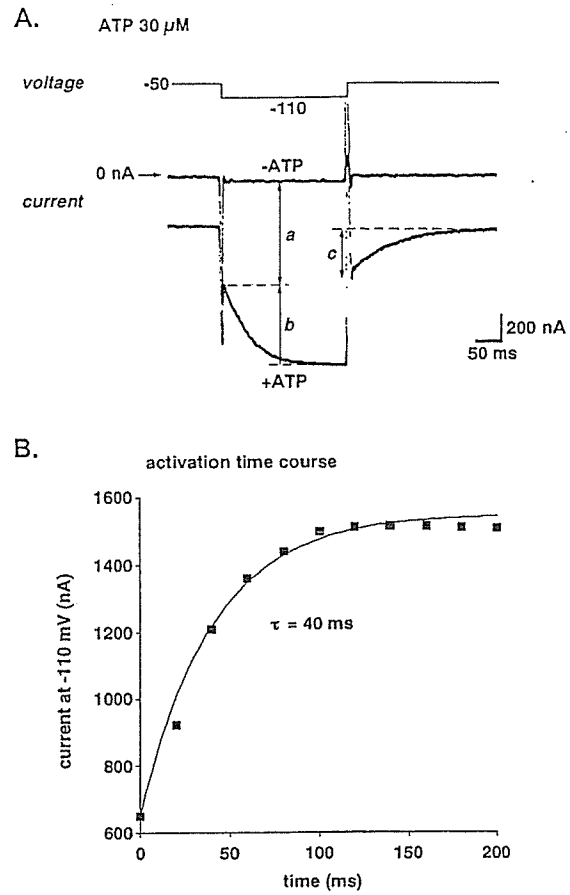

Fig. 1. (A) Current traces of an oocyte stepped to −110 mV from a holding potential of −50 mV in the absence (−ATP) or presence (+ATP) of 30 μM ATP. The current evoked by ATP is represented by the difference between the two traces. Upon hyperpolarization, a gradual increase in current was observed in the presence of ATP, suggesting activation of a voltage-dependent gate (denoted by "b"). The current denoted by "c" represents a gradually declining "tail current" that was observed when the voltage was returned to −50 mV. (B) Time course of activation of the voltage-dependent component. Current amplitude of the voltage-dependent component represented by "b" in panel A was plotted against time after the onset of hyperpolarization at −110 mV. The voltage-dependent component could be made to fit a curve with a time constant of 40 ms.

(Fig. 2C). While the current amplitude demonstrated voltage dependence (Fig. 2B), voltage did not have an effect on time course of the activation.

3.2. Effect of ATP concentrations

Fig. 3A shows the voltage-dependent component of the current activated by 10 μM or 300 μM of ATP in a single oocyte. The relative size of the voltage-dependent component involved in total ATP-evoked current became smaller when the current was evoked by greater concentrations of ATP (Fig. 3A and B). A similar dependence on ATP concentration was observed for the current evoked in the presence of 10.8 mM Ba^{2+} instead of 1.8 mM Ca^{2+} (Fig. 3B). Dependence on ATP concentrations was also found for activation time constants for the voltage-

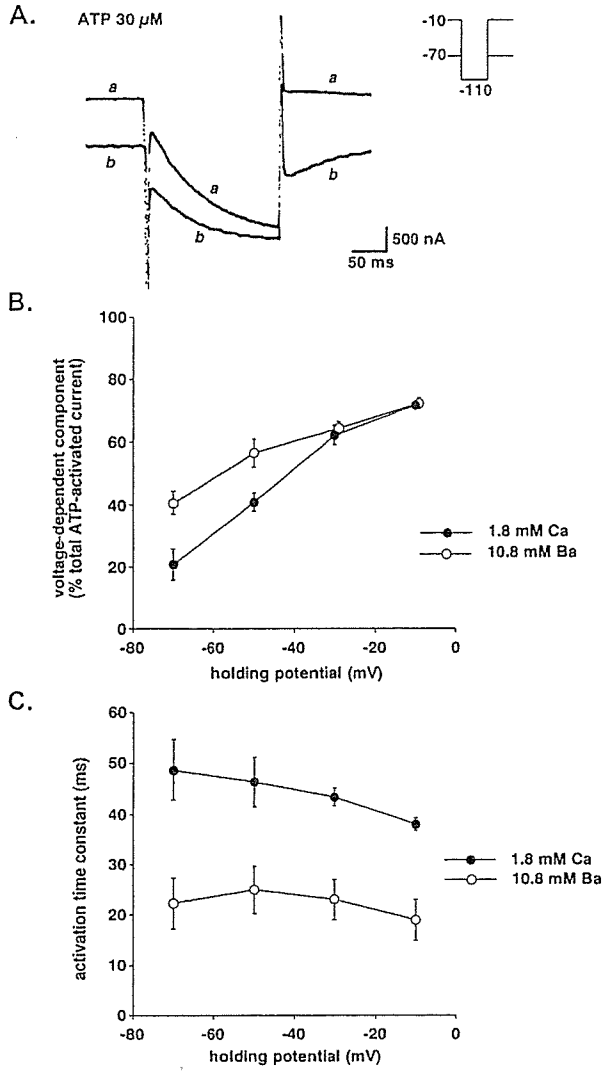

Fig. 2. Effect of holding potential on current. Current was evoked by 30 μM ATP. (A) Voltage-dependent current at −110 mV when stepped from a holding potential of −10 mV ("a") or −70 mV ("b"). (B) Effect of holding potential on voltage-dependent current. The amplitude of the voltage-dependent current was measured as described in Fig. 1A. Mean values obtained from 4 oocytes in a standard extracellular solution containing 1.8 mM Ca^{2+} (●) and an extracellular solution containing 10.8 mM Ba^{2+} (instead of Ca^{2+}; O) were plotted. Bars represent the S.E.M. (C) Time course of activation of the voltage-dependent component. Time constants were determined as shown in Fig. 1B, and mean values obtained from 4 oocytes were plotted against holding potentials. Bars represent the S.E.M.

dependent component; the time constants were larger for 10 μM ATP than 30 μM ATP (Fig. 3C).

3.3. Activation and deactivation kinetics

Cl^- currents are observed in *Xenopus* oocytes (Weber, 1999; Zhang and Hamill, 2000). In the following experiments, current measurements were made using an extracellular solution containing 96 mM Na-aspartate instead of NaCl in order to facilitate the analysis of the voltage-dependent component of ATP-evoked current by reducing Cl^- currents. In doing so, there was an obvious reduction in outward current upon depolarization, resulting in better voltage-clamp conditions. Using this extracellular solution, the EC_{50} value for ATP-activated current measured at −50 mV was about 40 μM, which was lower than the value obtained with the standard extracellular solution containing 96 mM NaCl (about 100 μM; Nakazawa and Ohno, 2004). Fig. 4 illustrates

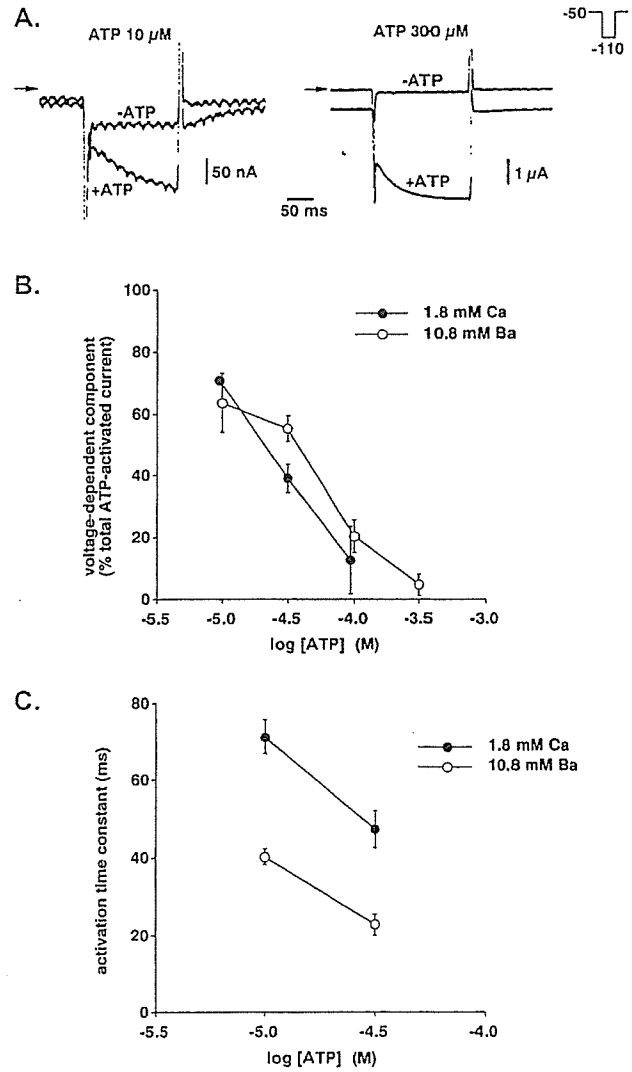

Fig. 3. Effect of ATP concentration. The voltage-dependent current was activated by hyperpolarization (−110 mV) from a holding potential of −50 mV. (A) Voltage-dependent current activated by 10 μM or 30 μM ATP. Current traces in the absence (−ATP) or presence (+ATP) of ATP are superimposed in each panel. (B) Contribution of the voltage-dependent current to total ATP-evoked current using different ATP concentrations. Mean values obtained from 4 oocytes in a standard extracellular solution containing 1.8 mM Ca^{2+} (●) and an extracelllular solution containing 10.8 mM Ba^{2+} (instead of Ca^{2+}; O) were plotted. Bars represent the S.E.M. (C) Time course of activation of the voltage-dependent components. Time constants were determined as shown in Fig. 1B, and mean values obtained from 4 oocytes were plotted against holding potentials. Bars represent the S.E.M.

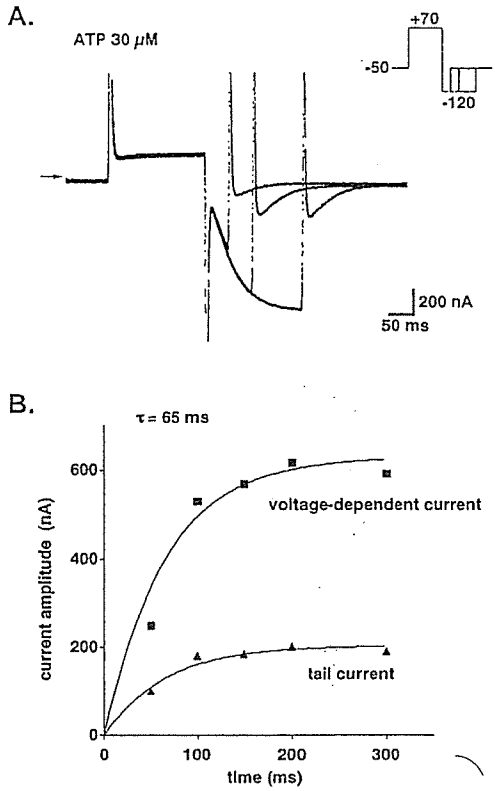

Fig. 4. Activation and tail current. (A) Gradual increase in magnitude of the tail current with increasing voltage-dependent current. Current traces obtained upon exposure to hyperpolarizing pulses (−120 mV) of different durations are superimposed. (B) Time course of activation of the voltage-dependent (■) and tail (▲) currents. Current amplitude was plotted against duration of hyperpolarization (also shown in panel A). The results of both time course activation experiments fit curves with a single time constant of 65 ms.

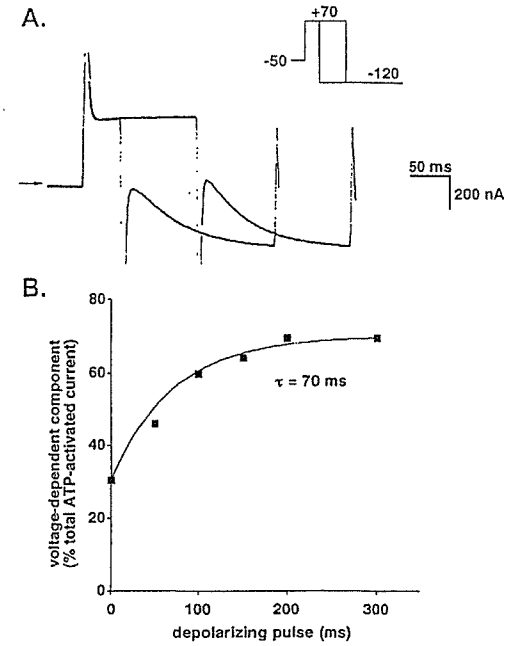

Fig. 5. Deactivation of the voltage-dependent component. (A) Current traces obtained using depolarizing pulses (+70 mV) of two different durations. The amplitude of the voltage-dependent component increased when the duration was prolonged. (B) Time course of deactivation of the voltage-dependent component. Current amplitude was plotted against duration of the depolarizing pulses (also shown in panel A).

the relation between activation kinetics of the voltage-dependent component and time course of tail current. As shown in Fig. 4A, oocytes were stepped to 70 mV and then to −120 mV to induce the voltage-dependent component. When hyperpolarization at −120 mV was terminated after various periods, a gradual increase in amplitude of the tail current was observed with increased duration of hyperpolarization at −120 mV. Time courses of both the voltage-dependent component and tail current could be fitted with curves with a single time constant (65 ms in this case; Fig. 4B). Similar fitting with single time constants were made for 4 oocytes tested, and the mean time constant±S.E.M. was 66.3±2.4 ms.

With increased duration of the +70 mV depolarizing pulse, increased amplitude of the voltage-dependent component was observed at −120 mV (Fig. 5A). This may reflect "deactivation" of the voltage-dependent component (Scheme 1):, where A is ATP, and R and R* are closed and open states, respectively, of the voltage-dependent component of $P2X_2$ receptor/channel. The deactivation time course could be fitted with a time constant of 70 ms in this case (Fig. 5B; mean±S.E.M., 71.3±1.3 ms; n=4).

3.4. Voltage dependence of activation and deactivation

As shown in Fig. 1, contribution of the voltage-dependent component to total ATP-evoked current was influenced by the holding potential prior to hyperpolarization. This was further examined by testing a number of prepulses at various potentials prior to hyperpolarization (Fig. 6A). As the prepulse became more depolarized, a greater contribution of the voltage-dependent component to total ATP-evoked current was observed, and this contribution became maximal near 0 mV (Fig. 6B). Thus, the voltage-dependent gate must be completely closed at potentials equal to or more positive than 0 mV. The data were fitted with a curve in accordance with the following model of "deactivation":

$$d_\infty = 1/\{1 + \exp[(E_{1/2} - E_m)/k]\}, \quad (1)$$

where d_∞ represents the relative proportion of closed gates at steady state, $E_{1/2}$ is the voltage at which the half-maximal closing occurs, E_m is the membrane potential, and

$$A{\cdot}R \underset{\text{(deactivation)}}{\overset{\text{(activation)}}{\rightleftharpoons}} A{\cdot}R^*$$

Scheme 1.

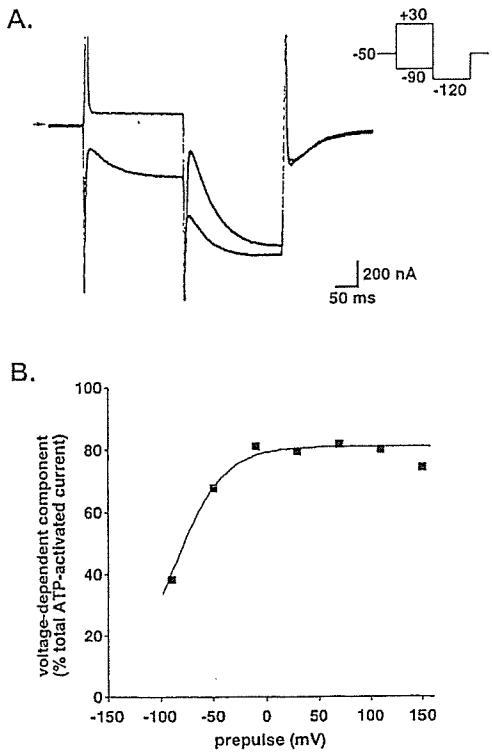

Fig. 6. Prepulse experiment. An ATP concentration of 30 μM was used. (A) Current traces obtained using prepulses of +30 mV ("a") or −90 mV ("b") prior to hyperpolarization at −120 mV. (B) Effect of prepulses. The relative contribution of the voltage-dependent current to total ATP-evoked current at −120 mV was plotted against each prepulse voltage. Some of this data is also shown in panel A.

k is a slope factor reflecting an energy barrier (Hodgkin and Huxley, 1952; Hille, 1992a). As shown in Fig. 6B, potential at which half the gates closed was estimated to be −90 mV in this case (mean±S.E.M., −78.8±5.2 mV; n=4).

The voltage dependence of activation was also examined. As shown in Fig. 7A, the channels responsible for the voltage-dependent component was sufficiently "deactivated" by applying a prepulse of +100 mV, and they were then activated at various hyperpolarization potentials. Contribution of the voltage-dependent component to total ATP-evoked current decreased as the hyperpolarization became more negative up to −45 mV in the case shown in Fig. 7B. Potentials exceeding −45 mV could not be examined since the resultant ATP-evoked current was not large enough to analyze. The data were fitted in accordance with the following model of "activation":

$$a_\infty = 1/\{1+\exp[(E_{1/2}-E_m)/k]\}, \quad (2)$$

where a_∞ represents the degree of gate opening at steady state. The other parameters are the same as those described above. The data obtained using Eq. (2) (Fig. 7B) could be fitted with a curve indicating that half of the gates were open at a potential of −30 mV.

The above data suggest that activation of the voltage-dependent gate occurs at more positive potentials than gate deactivation. To further investigate this, the fraction of the gates that escaped deactivation ($1-d_\infty$) was calculated from the data obtained during deactivation experiments. The deactivation data was then plotted alongside data obtained from activation experiments (Fig. 7C). These data suggest that the activation potential is 50 mV more positive than the deactivation potential.

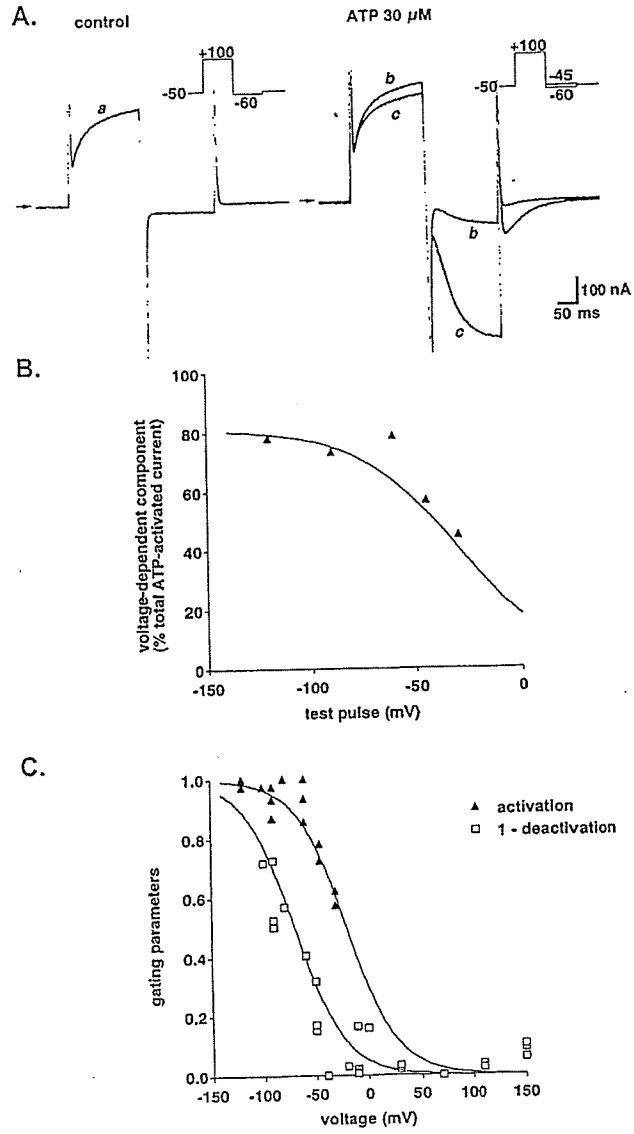

Fig. 7. Effect of hyperpolarization on voltage-dependent current. (A) Current traces before (control) and during the application of 30 μM ATP. In the panel on the right, two current traces obtained following hyperpolarization at −45 mV ("b") and −60 mV ("c") are superimposed. (B) Contribution of voltage-dependent current to total ATP-evoked current at various hyperpolarization potentials. Some of these data are shown in panel A. (C) Comparison of activation and deactivation. Parameters describing activation and deactivation were determined as described in the text. Each data point represents data obtained from individual oocytes.

4. Discussion

4.1. Schematic model of voltage-dependent gating

Recombinant $P2X_2$ receptor/channels expressed in *Xenopus* oocytes exhibited voltage-dependent gating properties similar to those of the channels in PC12 cells (Nakazawa et al., 1997b). The following similarities were observed: (1) the gate opens at negative potentials, (2) activation follows a time course with a time constant of 40 to 70 ms, and (3) gating depends on ATP concentrations. Thus, voltage-dependent gating in PC12 cells may be due to intrinsic expression of $P2X_2$ receptor/channels. We depict here a model that has been proposed to explain voltage-dependent gating of the channels in PC12 cells (Scheme 2):, where A is ATP, R_L and R_H represent closed states, and R* represents the open state (Nakazawa et al., 1997b). In this model, voltage-dependent gating is explained by transition between low and high ATP-affinity states. Upon hyperpolarization, there is a shift from the R_L to the R_H conformation. ATP preferentially binds to channels in the R_H state ($A \cdot R_H$), after which the channels open ($A \cdot R_H^*$). Binding of ATP is the rate-limiting step since activation kinetics were observed to depend on ATP concentrations in the present study (Fig. 3C). The following rate constants have been proposed (Scheme 3): where k_{+1} parallels the concentration of ATP ($k_{+1}=k'_{+1}$[ATP]), and K_d is given by k_{-1}/k'_{+1} (Hille, 1992b). In the present experiment, an activation time constant of 65 ms was observed in the presence of 30 μM of ATP (Fig. 4), which is equivalent to a rate constant of 15 s^{-1}. Using these values, $k'_{+1}=k_{+1}/[ATP]=15\ s^{-1}/(30\ \mu M)=5\times10^5\ M^{-1}\ s^{-1}$. An inactivation time constant of 70 ms was observed in the presence of 30 μM of ATP (Fig. 5), which is equivalent to a rate constant of 14 s^{-1}. Thus, K_d was calculated to be $k_{-1}/k'_{-1}=14\ s^{-1}/(5\times10^5\ M^{-1}\ s^{-1})=28$ μM, which is slightly less than the EC_{50} value obtained at −50 mV (about 40 μM). This estimation is in accordance with the finding that the voltage-dependent component is not completely activated at −50 mV (Fig. 7C). It is difficult to quantify the low-affinity ATP binding state since the relationship between concentration and response needs to be assessed at highly positive potentials, while $P2X_2$ receptor/channels permit only small current due to their inward-rectifying

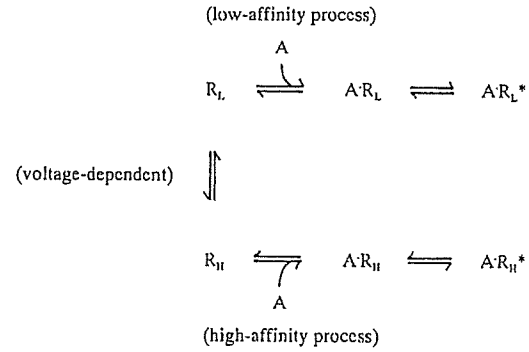

Scheme 2.

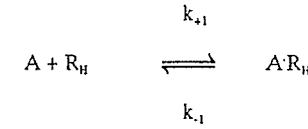

Scheme 3.

nature. We estimate here the low affinity from simple theoretical concentration–response curves. Fig. 8 shows two concentration–response curves. One demonstrates an EC_{50} of 30 μM, corresponding to a high-affinity state. If the other low-affinity state demonstrates an EC_{50} of 100 μM, more $P2X_2$ receptor/channels were in the high-affinity state in the presence of 10 μM ATP, and more were in the low-affinity state in the presence of 300 μM ATP. This is consistent with the greater observed contribution of the voltage-dependent component to total ATP-evoked current in the presence of 10 μM, while little was observed in the presence of 300 μM ATP (Fig. 3). Thus, the low-affinity state may be lower than the high-affinity state by threefold or larger.

The idea of the transition of $P2X_2$ receptor/channels between low- and high-affinity states might explain the "non-voltage-dependent" component of ATP-evoked current. For example, the current evoked by 30 μM ATP was not completely observed as voltage-dependent component even when activated at very negative potentials (Fig. 7B) or following deactivation at very positive potentials (Fig. 6B). This "non-voltage-dependent current" (about 20% of the total ATP-evoked current) might result from the activation of $P2X_2$ receptor/channels in the low-affinity state prior to voltage-dependent activation.

The voltage dependence of activation and deactivation differed, with deactivation occurring at more negative potentials (Fig. 7C). This indicates that the activation and the deactivation do not arise from a simple reversible "back-and-forth" process, rather, two voltage-dependent processes

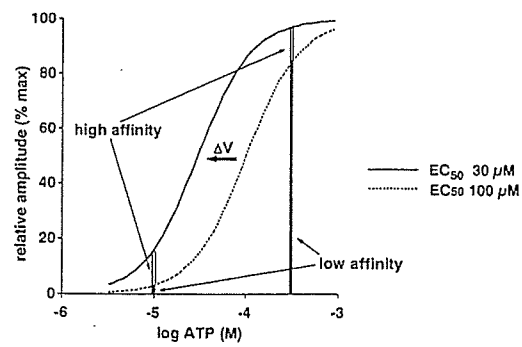

Fig. 8. Voltage-dependent change in sensitivity to ATP might explain dependence of the voltage-dependent current on ATP concentration. Low-affinity (EC_{50}=100 μM) and high-affinity (EC_{50}=30 μM) states of the receptor are thought to exist (Hill coefficient; 1.5). Each receptor shifts from a low-affinity to a high-affinity state upon hyperpolarization (ΔV). With 10 μM ATP, only a small proportion of the receptors, many of which were in the low-affinity state, were activated prior to hyperpolarization, but many more were activated upon induction of the high-affinity state by hyperpolarization. In the presence of 300 μM ATP, a larger proportion of the receptors were activated even in the low-affinity state, and induction of the high-affinity state caused only a marginal increase in activated receptors.

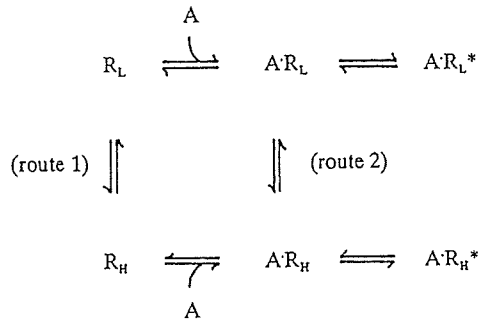

Scheme 4.

may be involved. We propose the following modification to Scheme 2.

This model (Scheme 4) involves two voltage-dependent processes, one resulting in activation through "route 1", and the other resulting in deactivation through "route 2". Such model would explain the observed difference in voltage dependence between activation and deactivation. However, we would expect this model to result in more difficult to interpret data than we did above based on Schemes 2 and 3.

4.2. Relevance of voltage-dependent gating

$P2X_2$ receptor is expressed in a number of neurons (e.g., Atkinson et al., 2000; Rubio and Soto, 2001). $P2X_2$ receptor/channel is permeable to Ca^{2+} (Egan and Khakh, 2004), and Ca^{2+} influx through the channel may influence cellular activity, although its exact role remains to be clarified. The voltage-dependent gating reported here may be relevant to the Ca^{2+} influx from the following consideration. Na^+ current (I_{Na}) and Ca^{2+} current (I_{Ca}) permeating through $P2X_2$ receptor/channel are:

$$I_{Na} = -P_{Na}\frac{E_m F^2}{RT}\frac{[Na]_o}{1-\exp(-EF/RT)} \quad (3)$$

$$I_{Ca} = -4P_{Ca}\frac{E_m F^2}{RT}\frac{[Ca]_o \exp(-2EF/RT)}{1-\exp(-2EF/RT)}, \quad (4)$$

where P_{Na} and P_{Ca} represent the permeability of Na^+ and Ca^{2+}, respectively, E_m represents the membrane potential, and F, R, and T are their usual physicochemical meanings (Fatt and Ginsborg, 1958; Nakazawa et al., 1989). The ratio of I_{Na} to I_{Ca} is thus:

$$\frac{I_{Ca}}{I_{Na}} = \frac{4P_{Ca}[Ca]_o}{P_{Na}[Na]_o}\frac{1}{\exp(E_m F/RT)[\exp(E_m F/RT)+1]} \quad (5)$$

This equation indicates that the ratio of I_{Ca}/I_{Na} is larger at more negative potentials. The ratio calculated at −90 mV is about 13-fold larger than that calculated at −30 mV. Thus, channel opening at negative potentials favors Ca^{2+} over Na^+ influx. Thus, voltage-dependent gating may facilitate cellular Ca^{2+}-dependent responses when cells are hyperpolarized. This may occur when efflux through K^+ channels outpaces depolarization afforded by opening of $P2X_2$ receptor/channels.

4.3. Conclusion

The results of the present study suggested that $P2X_2$ receptor exhibits voltage-dependent gating, and that this is not due to simple activation and deactivation of a single gate, but rather, due to a transition from a low ATP affinity to a high ATP affinity state. This may favor Ca^{2+} influx at negative potentials, although further studies are required to clarify the physiological significance of voltage-dependent gating of $P2X_2$ receptor.

Acknowledgements

This work was supported, in part, by a Health and Labour Science Research Grant for Research on Advanced Medical Technology from the Ministry of Health, Labour and Welfare, Japan, as well as a grant-in-aid for scientific research from the Ministry of Education, Science, Sports and Culture, Japan (KAKENHI 13672319) awarded to K.N.

References

Atkinson, L., Batten, T.F., Deuchars, J., 2000. $P2X_2$ receptor immunoreactivity in the dorsal vagal complex and area postrema of the rat. Neuroscience 99, 683–696.

Brake, A.J., Wagenbach, M.J., Julius, D., 1994. New structural motif for ligand-gated ion channels defined by an ionotropic ATP receptor. Nature 371, 519–523.

Clyne, J.D., LaPointe, L.D., Hume, R.I., 2002. The role of histidine residues in modulation of the rat $P2X_2$ purinoceptor by zinc and pH. J. Physiol. 539, 347–359.

Egan, T., Khakh, B.S., 2004. Contribution of calcium ions to P2X channel responses. J. Neurosci. 24, 3413–3420.

Egan, T.M., Haines, W.R., Voigt, M.M., 1998. A domain contributing to the ion channel of ATP-gated $P2X_2$ receptors identified by the substituted cysteine accessibility method. J. Neurosci. 18, 2350–2359.

Ennion, S., Hagan, S., Evans, R.J., 2000. The role of positively charged amino acids in ATP recognition by human $P2X_1$ receptors. J. Biol. Chem. 275, 29361–29367.

Fatt, P., Ginsborg, B.L., 1958. The ionic requirements for the production of action potentials in crustacean muscle fibres. J. Physiol. 142, 516–543.

Haines, W.R., Migita, K., Cox, J.A., Egan, T.M., Voigt, M.M., 2001. The first transmembrane domain of the P2X receptor subunit participates in the agonist-induced gating of the channel. J. Biol. Chem. 276, 32793–32798.

Hille, B., 1992a. Classical biophysics of the squid giant axon. Ionic channels of excitable membranes, Second Edition. Sinauer, Sunderland, MA, pp. 23–58.

Hille, B., 1992b. Ligand-gated channels of fast chemical synapses. Ionic channels of excitable membranes, Second Edition. Sinauer, Sunderland, MA, pp. 140–169.

Hodgkin, A.L., Huxley, A.F., 1952. The dual effect of membrane potential on sodium conductance in the giant axon of *Loligo*. J. Physiol. 116, 497–506.

Jiang, L.H., Rassendren, F., Surprenant, A., North, R.A., 2000. Identification of amino acid residues contributing to the ATP-binding site of a purinergic P2X receptor. J. Biol. Chem. 275, 34190–34196.

Jiang, L.H., Rassendren, F., Spelta, V., Surprenant, A., North, R.A., 2001. Amino acid residues involved in gating identified in the first membrane-spanning domain of the rat $P2X_2$ receptor. J. Biol. Chem. 276, 14902–14908.

Khakh, B.S., 2001. Molecular physiology of P2X receptors and ATP signalling at synapses. Nat. Rev. 2, 165–174.

Migita, K., Haines, W.R., Voigt, M.M., Egan, T.M., 2001. Polar residues of the second transmembrane domain influence cation permeability of the ATP-gated $P2X_2$ receptor. J. Biol. Chem. 276, 30934–30941.

Nakazawa, K., Ohno, Y., 1997. Effects of neuroamines and divalent cations on cloned and mutated ATP-gated channels. Eur. J. Pharmacol. 325, 101–108.

Nakazawa, K., Fujimori, K., Takanaka, A., Inoue, K., 1989. An ATP-activated conductance in pheochromocytoma cells and its suppression by extracellular calcium. J. Physiol. 428, 257–272.

Nakazawa, K., Liu, M., Inoue, K., Ohno, Y., 1997a. pH dependence of facilitation by neurotransmitters and divalent cations of $P2X_2$ purinoceptor/channels. Eur. J. Pharmacol. 337, 309–314.

Nakazawa, K., Liu, M., Inoue, K., Ohno, Y., 1997b. Voltage-dependent gating of ATP-activated channels in PC12 cells. J. Neurophysiol. 78, 884–890.

Nakazawa, K., Ojima, H., Ohno, Y., 2002. A highly conserved tryptophane residue indispensable for cloned rat neuronal P2X receptor activation. Neurosci. Lett. 324, 141–144.

North, R.A., 2002. Molecular physiology of P2X receptors. Physiol. Rev. 82, 1013–1067.

North, R.A., Surprenant, A., 2000. Pharmacology of cloned P2X receptors. Annu. Rev. Pharmacol. Toxicol. 40, 563–580.

Ralevic, V., Burnstock, G., 1998. Receptors for purines and pyrimidines. Pharmacol. Rev. 50, 413–492.

Rassendren, F., Buell, G., Newbolt, A., North, R.A., Surprenant, A., 1997. Identification of amino acid residues contributing to the pore of a P2X receptor. EMBO J. 16, 3446–3454.

Roberts, J.A., Evans, R.J., 2004. ATP binding at human $P2X_1$ receptors. Contribution of aromatic and basic amino acids revealed using mutagenesis and partial agonists. J. Biol. Chem. 279, 9043–9055.

Rubio, M., Soto, F., 2001. Distinct localization of P2X receptors at excitatory postsynaptic specializations. J. Neurosci. 21, 641–653.

Weber, W.-M., 1999. Ion currents of *Xenopus laevis* oocytes: state of the art. Biochim. Biophys. Acta 1421, 213–233.

Zhang, Y., Hamill, O.P., 2000. Calcium, voltage- and osmotic stress sensitive currents in *Xenopus* oocytes and their relationship to single mechanically gated channels. J. Physiol. 523, 83–99.

Available online at www.sciencedirect.com

SCIENCE DIRECT®

European Journal of Pharmacology 518 (2005) 107 – 110

www.elsevier.com/locate/ejphar

Short communication

Purification and aqueous phase atomic force microscopic observation of recombinant $P2X_2$ receptor

Ken Nakazawa [a,*], Yoko Yamakoshi [b,1], Toshie Tsuchiya [c], Yasuo Ohno [a]

[a] *Division of Pharmacology, National Institute of Health Sciences, 1-18-1 Kamiyoga, Setagaya, Tokyo 158-8501, Japan*
[b] *Division of Organic Chemistry, National Institute of Health Sciences, 1-18-1 Kamiyoga, Setagaya, Tokyo 158-8501, Japan*
[c] *Division of Medical Devices, National Institute of Health Sciences, 1-18-1 Kamiyoga, Setagaya, Tokyo 158-8501, Japan*

Received 4 April 2005; received in revised form 14 June 2005; accepted 20 June 2005
Available online 28 July 2005

Abstract

Recombinant $P2X_2$ receptor was observed by atomic force microscope in the aqueous phase. The $P2X_2$ receptor was expressed in an insect cell line, and recombinant proteins were prepared under native conditions. The membrane fractions were extracted, and histidine-tagged receptor protein was purified from the fractions by column chromatography. When the purified protein fraction was diluted with water and served for atomic force microscopy, dispersed particles of about 3 nm in height were observed. In the presence of 1 mM ATP, the assembly-like images of the particles were obtained. More densely assembled images of the particles were achieved when the protein was dissolved in a Tris buffer containing 1 mM ATP. Under this condition, imaging of the surface of the particles exhibited a circular structure with a diameter of about 10 nm having a pore-like structure. These results suggest that atomic force microscopy provides structural information about $P2X_2$ receptor in aqueous phase.

Keywords: P2X receptor; Atomic force microscopy; Protein structure; ATP

1. Introduction

P2X receptors are ion channel forming membrane proteins that are activated by extracellular ATP, and their physiological roles have been shown in various tissues including the central nervous system (see reviews, Khakh, 2001; North, 2002; Vial et al., 2004). This ion channel/receptor family consists of 7 subclasses ($P2X_1$ to $P2X_7$), and is believed to have molecular structures distinct from so-called "ligand-gated channel super family" including nicotinic acetylcholine receptor/channels and ionotropic glutamate receptor channels. Structural analyses such as the X-ray crystal analysis have not been made for P2X receptor/channel family. In addition, because of their distinct structures, estimation from homology modeling based on known three-dimensional structures of other proteins is difficult. Thus, information concerning the structure and morphology of P2X receptor is lacking. Atomic force microscopy is an approach for structural analysis that allows the analysis of a small amount (nanogram to microgram) of uncrystalized protein. Atomic microscopy enables the observation of both individual and assembled protein molecules in the aqueous phase, which may reveal dynamic forms of biologically active proteins (Müller and Engel, 2002). Recently, Barrera et al. (2005) reported atomic force microscopy imaging of dried P2X receptor protein. In the present study, we have prepared $P2X_2$ receptor protein from an insect cell line expression system, and made atomic force microscopy imaging in aqueous phase. The imaging has revealed that $P2X_2$ receptor is a pore-forming protein for the first time.

* Corresponding author. Tel.: +81 3 3700 9704; fax: +81 3 3707 6950.
E-mail address: nakazawa@nihs.go.jp (K. Nakazawa).
[1] Present address: Center for Polymers and Organic Solids, Department of Chemistry and Biochemistry, University of California, Santa Barbara, CA 93106-9510, USA.

0014-2999/$ - see front matter © 2005 Elsevier B.V. All rights reserved.
doi:10.1016/j.ejphar.2005.06.018

2. Materials and methods

2.1. Preparation of recombinant $P2X_2$ receptor protein

N-terminal hexahistidine-tagged recombinant rat $P2X_2$ receptor was expressed using baculovirus-Sf9 system, which has been used for the expression of membrane receptor proteins (e.g., Boundy et al., 1993; Ng et al., 1993). cDNA encoding rat $P2X_2$ receptor (Brake et al., 1994) was subcloned into pFast BAC HTc vector (BD Bioscience Clonetech, Palo Alto, CA, USA). The recombinant virus was transfected to insect-derived clonal Sf9 cells. After culturing at a volume of 500 ml at room temperature, the culture medium was centrifuged at 130 $\times g$ for 5 min, and the precipitated cells were washed with Ca^{2+}, Mg^{2+}-free phosphate buffered saline (137 mM NaCl, 2.7 mM KCl, 8.1 mM Na_2HPO_4, and 1.5 mM KH_2PO_4; PBS(−)) twice. The cells were then suspended in a Tris–HCl (pH 7.4) lysis buffer containing Triton X-100, and homogenized. NaCl was added such that its final concentration became 100 mM. This solution was centrifuged at 30000 $\times g$ for 20 min, and the supernatant was then centrifuged at 380000 $\times g$ for 10 min. Polyacrylamide gel electrophoresis followed by immunoblotting analysis with anti-hexahistidine antibody showed that hexahistidine-tagged proteins of an expected size (56 kD) were found in this supernatant. Further purification was made using Chelating Sepharose FF colums. Ni^{2+}-bound columns were equilibrated with a buffer containing 20 mM Tris–HCl and 0.5 M NaCl (pH 8.0), and samples were applied. The bound receptor proteins were eluted by stepwise increase of imidazole (10, 20, 50, 100, 200 and 500 mM). The concentrations of the receptor protein in the eluted solutions were estimated by measuring absorbance at 595 nm. The most purified $P2X_2$ receptor protein (>90% of total protein) was found in the fraction eluted by 10 mM imidazole, and this fraction was served for atomic force microscopy imaging. The purified $P2X_2$ receptor exhibited the ability to bind ATP when photoaffinity labeling with [α-^{32}P]ATP was performed according to Kim et al. (1997). In this experiment, the binding of [α-^{32}P]ATP was markedly reduced by 100 μM nonradiolabeled ATP.

2.2. Atomic force microscopy imaging

The protein solution (about 1.5 μM) was diluted to appropriate concentrations (0.1 to 10 nM) with water, and the diluted solution was placed on freshly cleaved mica. After 30 min, unbound proteins were washed away with water, and served for atomic force microscopy imaging. When ATP (disodium salt; Sigma, St. Louis, MO, USA) was added to water, 1 mM solution was neutralized to pH 7.4 with 2 N NaOH (final Na^+ concentration was about 16 mM). In part of the experiments, the protein solution was diluted with a Tris buffer of the following composition (in millimolar): Tris 50, KCl 150, $MgCl_2$ 10, dithiothreirol 1 (pH 7.0). This buffer composition was similar to that utilized for atomic force microscopy imaging of *Escherichia coli* GroES (Cheung et al., 2000). Imaging was made in an aqueous tapping mode using MFP-3D (Asylum Research, Santa Barbara, CA, USA) equipped with OMCL-TR800PSA (Olympus, Tokyo, Japan) as a probe.

3. Results

Fig. 1A shows atomic force microscopy images of purified $P2X_2$ receptor proteins in water. A larger part of the proteins were found as dispersed particles. The height of single $P2X_2$ receptor proteins was about 3 nm (Fig. 1B). In the presence of 1 mM ATP, larger particles, presumably clots of several receptor proteins, were observed in addition to dispersed particles (Fig. 1C). A flatly and densely assembled image was obtained when the proteins were dissolved in a Tris buffer containing 1 mM ATP (Fig. 2A). Densely packed assembly is advantageous for atomic force microscopy imaging because resolution is improved due to smaller movement of probes along Z-axis (Müller and Engel, 2002). When the protein assembly shown in Fig. 2A was imaged at higher magnification, a circular structure with a pore was observed (Fig. 2B). The diameter of the circular structure was about 10 nm, and that of the pore was several nanometers. Without ATP, the protein was not densely assembled and did not exhibit uniform direction (not shown).

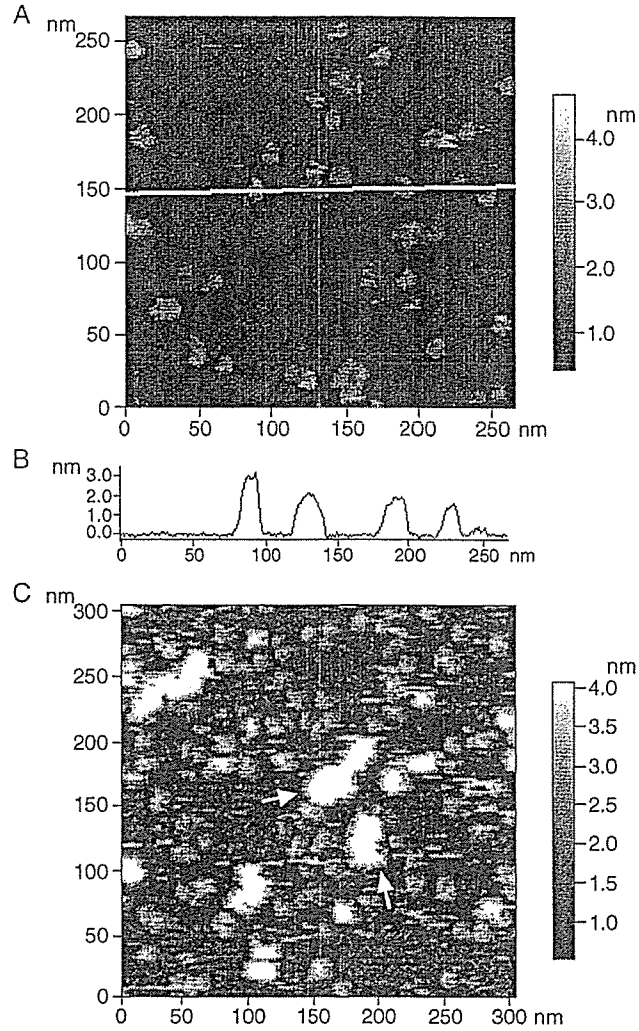

Fig. 1. (A) An atomic force microscopy image of $P2X_2$ receptor proteins in water. Isolated single receptor proteins and their small assemblies are seen. (B) A section of the image shown in (A). The section was made along with the line. The height of receptor proteins is about 3 nm or less. (C) An image of $P2X_2$ receptor proteins in the presence of 1 mM ATP. In addition to single receptor proteins, clots of the proteins (indicated by arrows) were also seen.

4. Discussion

For atomic force microscopy imaging of membrane proteins, densely expressed proteins in particular cells have

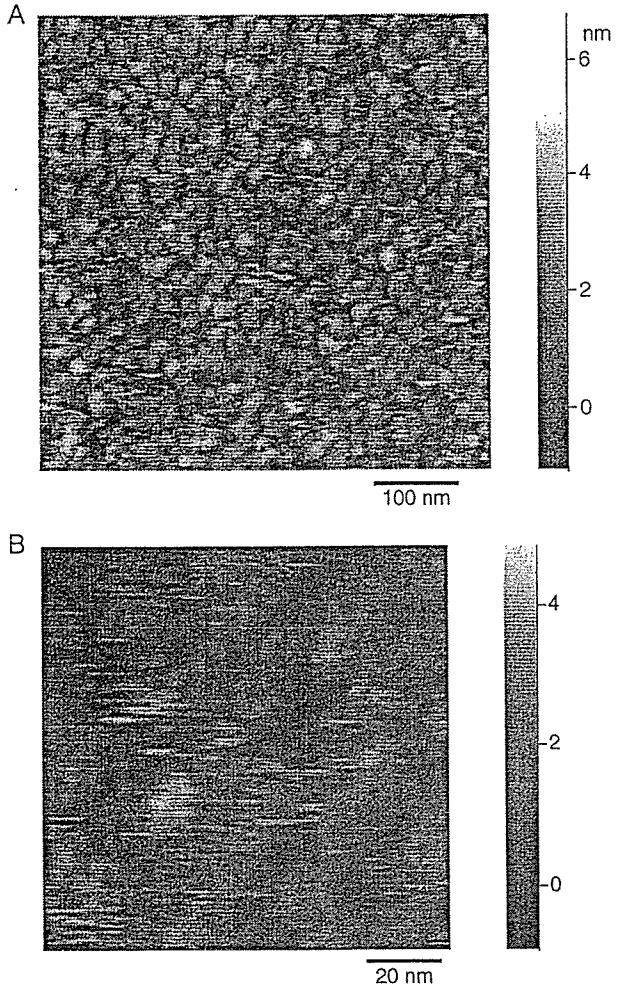

Fig. 2. (A) An image of $P2X_2$ receptor proteins in a Tris buffer containing 1 mM ATP. The proteins were flatly and densely assembled. (B) An expanded image. The upper surfaces of individual proteins exhibited a circular structure having a pore in its center.

been served in the presence of lipid bilayers (Müller and Engel, 2002; Müller et al., 2002). This two-dimensional (2D) protein crystal can provide high resolution of images, especially when combined with image processing including averaging. However, preparation of 2D crystals requires skilled techniques or special equipment. The present study has shown that recombinant $P2X_2$ can be imaged by atomic force microscopy without special techniques, but by simply adding agonist molecule, ATP. The role of ATP in promoting the densely packed assembly is unclear at present. It is speculated that receptor protein molecules without ATP freely move and exhibit various conformations, whereas ATP-bound receptor molecules exhibit only one or a restricted number of conformations in aqueous phase. The pore identified in the center of the protein may be the ion channel involved in $P2X_2$ receptor. A similar pore has been observed in connexin that also forms ion channels (Müller et al., 2002). It is unclear that the pore corresponds to the inner mouth or the outer mouth of the channel. Nevertheless, it is interesting that a number of proteins appear to exhibit similar surface structure (Fig. 2B). P2X receptor possesses a large extracellular domain, and, thus, it is possible that this domain is orientated upward to increase contact with the aqueous phase. Atomic force microscopy imaging of isolated membrane proteins may be less advantageous to elucidate biological functions compared to those embedded in lipid bilayer. However, isolated proteins are more readily observed than membrane preparations, and the imaging of these proteins may provide insights into the intrinsic properties of proteins and useful information to clarify the interactions between proteins and the membrane.

Barrera et al. (2005) observed dried $P2X_2$ receptor protein as a simple particle. We have revealed the outer structure of the protein, suggesting that resolution was better in the present study. However, our observation has not resolved trimeric assembly of $P2X_2$ receptor protein, which has been shown using antibodies specific for the protein (Barrera et al., 2005). Trimeric assembly of P2X receptor has been also demonstrated by electrophysiological and biochemical studies, and two transmembrane regions of each subunit are believed to contribute to the forming of channel pore (North, 2002; Vial et al., 2004). If $P2X_2$ receptor forms a six-barrel channel like connexin, this may account for a similar pore size (about several nanometers). Further improvement will be necessary to identify individual subunit proteins that form $P2X_2$ receptor and clarify more detailed structure by atomic force microscopy.

Acknowledgments

We are grateful to Dr. Jeffrey W. Bode of Department of Chemistry and Biochemistry, University of California, Santa Barbara for improving our manuscript. This work was partly supported by a Health and Labour Science Research Grant for Research on Advanced Medical Technology from the Ministry of Health, Labour and Welfare, Japan awarded to K.N., Y.Y. and T.T., and a grant-in-aid for scientific research from the Ministry of Education, Science, Sports and Culture, Japan (KAKENHI 13672319) awarded to K.N.

References

Barrera, N.P., Ormond, S.J., Henderson, R.M., Murrell-Langnado, R.D., Edwardson, J.M., 2005. AFM imaging demonstrates that $P2X_2$ receptors are trimers, but that $P2X_6$ receptor subunits do not oligomerize. J. Biol. Chem. 280, 10759–10765.

Boundy, V.A., Luedtke, R.R., Gallitano, A.L., Smith, J.E., Filtz, T.M., Kallen, R.G., Molinoff, P.B., 1993. Expression and characterization of the rat D3 dopamine receptor: properties and development of antibodies. J. Pharmacol. Exp. Ther. 264, 1002–1011.

Brake, A.J., Wagenbach, M.J., Julius, D., 1994. New structural motif for ligand-gated ion channels defined by an ionotropic ATP receptor. Nature 371, 519–523.

Cheung, C.L., Hafner, J.H., Lieber, C.M., 2000. Carbone nanotube atomic force microscopy tips: direct growth by chemical vapor deposition and application to high-resolution imaging. Proc. Natl. Acad. Sci., U. S. A. 97, 3809–3813.

Khakh, B.S., 2001. Molecular physiology of P2X receptors and ATP signalling at synapses. Nat. Rev. 2, 165–174.

Kim, M., Yoo, O.J., Choe, S., 1997. Molecular assembly of the extracellular domain of $P2X_2$, an ATP-gated ion channel. Biochem. Biophys. Res. Commun. 240, 618–622.

Müller, D.J., Engel, A., 2002. Conformations, flexibility, and interactions observed on individual membrane proteins by atomic force microscopy. Methods Cell Biol. 68, 257–298.

Müller, D.J., Hand, G.M., Engel, A., Soslinsky, G., 2002. Conformational changes in surface structures of isolated connexin 26 gap junctions. EMBO J. 21, 3598–3607.

Ng, G.Y., George, S.R., Zastawny, R.L., Caron, M., Bouvier, M., Dennis, M., O'Dowd, B.F., 1993. Human serotonin 1B receptor expression in Sf9 cells: phosphorylation, palmitoylation, and adenylyl cyclase inhibition. Biochemistry 32, 11727–11733.

North, R.A., 2002. Molecular physiology of P2X receptors. Physiol. Rev. 82, 1013–1067.

Vial, C., Roberts, J.A., Evans, R.J., 2004. Molecular properties of ATP-gated P2X receptor ion channels. Trends Pharmacol. Sci. 25, 487–493.

In vitro study on the osteogenesis of normal human osteoblasts cultured on the discs of various kinds of calcium phosphate ceramics

Masato Tamai[1, a], Ryusuke Nakaoka[1,b] and Toshie Tsuchiya[1,c]

[1]Division of Medical Devices, National Institute of Health Science

1-18-1 Kamiyoga, Setagaya-ku, Tokyo 158-8501 Japan

[a]m-tamai@nihs.go.jp, [b]nakaoka@nihs.go.jp, [c]tsuchiya@nihs.go.jp

Keywords: Calcium phosphate ceramics, osteogenesis, cytotoxicity,

Abstract. We estimated effects of various CP ceramics on the properties of normal human osteoblasts (NHOst) as well as a viability of V79 fibroblasts. In the present study, five kinds of CP ceramics, namely, hydroxyapatite (HAp) flouroapatite (FAp), α-tricalcium phosphate (α-TCP), β-tricalcium phosphate (β-TCP) and tetracalcium phosphate (TTCP), were tested. Cytotoxicity test was carried out using V79 fibroblasts by colony assay system. The amounts differentiation level of NHOst was estimated from alkaline phosphatase (ALP) activity and osteocalcin.
From the results of colony assay, FAp and α-TCP showed strong cytotoxicities on V79 cells. The results from the proliferation studies of NHOst with CP ceramics were consistent with the results of colony assay. In addition, the ALP activities of NHOst with CP ceramics after 1week culture were significantly suppressed in comparison with that of NHOst alone. The osteocalcin amounts produced from NHOst cultured on β-TCP was the highest among five kinds of CP ceramics.

Introduction

Calcium phosphate (CP) ceramics have been studied to utilize as the scaffolds for repairing bone defects. For instance, hydroxyapatite ($Ca_{10}(PO_4)_6(OH)_2$, HAp) or β-tricalcium phosphate (β-$Ca_3(PO_4)_2$, β-TCP), can be biologically bonded to natural bones and their porous materials are effective for restoration of bone defects [1]. Fluoroapatite ($Ca_{10}(PO_4)_6F_2$, FAp) has been reported to have a potential of novel bone repairing materials with high stability *in vivo*, since solubility of FAp is lower than that of HAp [2]. In addition, CP cement is also promising for bone repair and it is well known that α-tricalcium phosphate (α-$Ca_3(PO_4)_2$, α-TCP) or tetracalcium phosphate ($Ca_4(PO_4)_2O$, TTCP) are starting materials for the harden reaction of the bone cement [3].

To develop biomaterials for utilizing for bone tissue, various properties, e.g. biological, physical or chemical property, should be satisfied. Among them, biological safety and osteogenesis properties, e.g. proliferation and differentiation of the osteoblasts, should be important factors to provided to the biomaterials. However, understandings of the biological interaction between osteoblasts and various CP ceramics are few, since the interaction has not been studied under the same experimental condition in detail. Therefore, we estimated effects of various CP ceramics on the properties of normal human osteoblasts (NHOst) as well as a viability of V79 fibroblasts in this study.

Materials and Methods

Materials

Cytotoxicity and osteogenesis of NHOst on five kinds of CP ceramics, namely, HAp, FAp, α-TCP, β-TCP and TTCP (Wako chem. Co. Ltd., Tokyo, Japan), were evaluated. 0.25g of CP powders was put into stainless mold and uniaxially pressed at 30MPa for 1 min to form pellets. The dimensions of the obtained CP pellet were 1mm in thickness and 12mm in diameter. CP pellets were sterilized by the autoclave 121°C for 20 min.

Cytotoxicty test on CP ceramics

Cytotoxicity test was carried out using Chinese hamster V79 lung fibroblasts by the colony assay system. V79 cells were maintained in Eagle's minimum essential medium (Nissui Pharmaceutical Co. Ltd.,) with 10% fetal calf serum (FCS, Intergen company) and incubated at 37 °C in a humidified atmosphere with 5% CO_2.

The method of cell seeding was shown below; At first, each CP pellets were placed in each culture wells of 24 well culture plates (Corning Co. Ltd.) and 300μl of culture medium was added into each well. Next, 50 cells/300μl of culture medium was added into each well and incubated for 4 h at 37°C. Finally, 400μl of culture medium was added and incubated at 37 °C in a humidified atmosphere with 5 % CO_2 for 7days.

In order to investigate the cell adhesive property on the CP ceramics, the culture medium was changed after cultivations for 4 h and incubated for 7days. The removed culture medium was transferred to another well of the plate and incubated for 7days as well.

Cytotoxicity of extracts from CP ceramics was also investigated in this study. Suspensions of CP ceramics in the culture medium (100mg/mL) were stirred at 37°C for 3days in 150rpm. The suspensions were centrifuged and the supernatants were collected to use as test extracts. The cytotoxicity test was carried out culturing 50 V79 cells in 1ml of the extracts and incubated at 37 °C for 7days.

After 7days, the cells were fixed in methanol and the number of the V79 colonies was counted after staining cells with 5%-Giemsa solution. In addition, the pH of the medium after 7-days culture was measured to estimate effect of the pH of the medium on the cytotoxicity test.

Osteogenesis evaluation of NHOst cultured on CP ceramics

NHOst were purchased from BioWhittaker Inc.(Walkersville,MD). The NHOst were maintained in alpha minimum essential medium (αMEM, Gibco, Grand Island, NY) containing 10%-FCS. incubators at 37 °C in a humidified atmosphere with 5% CO_2. All assays were performed using αMEM containing 10%-FCS supplemented with 10mM beta-glycerophosphate. Similar to the method of the cytotoxicity test, each CP pellets were placed in 24-well culture plates (Corning Co. Ltd.) and 300μl of culture medium was added into each well, followed by addition of 1ml of cell suspension (4×10^4 cells/ml) into each well.

Proliferation of NHOst cells cultured on various kinds of CP ceramics was estimated by Tetracolor One assay (Seikagaku Co., Ltd. Tokyo, Japan), which incorporates an oxidation reduction indicator based on detection of metabolic activity. After 7-days incubation, 2%-TetraColor One/αMEM solution was added to each well, followed by 2h incubation. The absorbance of the supernatant at 450nm was estimated using μQuant spectrophotometer (Bio-tek Instrument, Inc., Winooski, VT). After estimating the proliferation, the cells were washed by phosphate–buffered saline (PBS(-)), followed by addition of 1ml of 0.1M glycine buffer (pH=10.5) containing 10mM $MgCl_2$, 0.1mM $ZnCl_2$ and 4mM p-nitrophenylphosphate sodium salt. After incubating at room temperature for 5min, the absorbance of 405 nm of glycine buffer was detected using μQuant spectrophotometer to evaluated alkaline phosphatase (ALP) activity of the test cells. The amount of Osteocalcin produced by NHOst was evaluated using Gla-type Osteocalcin EIT kit (Takara. Co., Ltd.). The structural change of CP before and after autoclave sterilization or culture were investigated by powder X-ray diffraction (XRD) analysis and scanning electron microscopy(SEM). XRD analysis was carried out (Rigaku Co., Ltd. / RINT 2000) with the CuK_α radiation at 40kV, 50mA. SEM observations were performed (JEOL / JSM-5800LV) with an accelerating voltage of 25kV.

Results

Cytotoxicity of various CP ceramics

The results of the cytotoxicity test of CPs are summarized in table 1. Notably, the colonies were hardly formed on FAp and α-TCP pellets and the ratios of the colony formation against V79-alone culture were 22.6% and 0.0%, respectively. In addition, the ratios of the colony formation on the HAp, β-TCP and TTCP pellets were 58.1%, 57.3% and 78.4%, respectively. From these results, it is suggested that V79 cells were viable and adhered on the pellet after for 4h after seeding despite of the type of CP ceramics, irrespective of the type of CP ceramics. On the other hand, the cytotoxicity test of extracts from CPs revealed that the tendency of their cytotoxicity was almost the same as that of the respective CP pellets themselves (table1).

Proliferation and differentiation of NHOst cultured on CP ceramics

The effects of various kinds of CP ceramics on the osteogenesis of NHOst are represented in table2. The effects of the CPs on proliferation were consistent with those on the colony formation. Similar to the cytotoxicity test, the proliferation of NHOst was inhibited on FAp and α-TCP pellets. ALP activities of NHOst on CP ceramics after 7-days culture were significantly suppressed in comparison with that of NHOst alone. On the other hand, the osteocalcin amounts produced from NHOst were influenced by the type of CP ceramics. NHOst on β-TCP showed the highest Osteocalcin production among five kinds of CP ceramics.

4. Discussion

The fact that less formation of colonies was observed on FAp and α-TCP pellets suggests that they are strongly cytotoxic. It is suggested that the differences in the colony formation on various CP pellets are ascribed to difference in extract properties from the CP related with the composition or crystal structure (table1). In addition, proliferation of NHOst also was inhibited on FAp and α-TCP. The pH values of culture medium after incubation for 7 days are shown in table1. As shown in the table, the pH of culture medium after incubation with FAp pellets is almost the same as that of HAp, while the pH of the α-TCP medium is much lower than other CP ceramics. In order to considering the reason of the low pH of the culture medium with α-TCP pellet, a surface structural change of α-TCP before and after incubation was analyzed by SEM. SEM images of α-TCP after extraction treatment are shown in Fig.1.

Table1. Cytotoxicity test of various CP ceramics.

Samples	Composition	Formation of colony		pH of medium after culturing	Ca concentration[1] /ppm
		On pellets /%	Extraction / %		
V79 alone	-	100.0±4.5	100.0±13.9	7.12	-
HAp	$Ca_{10}(PO_4)_6(OH)_2$	58.1±12.8	84.6±15.1	7.24	0.19
FAp	$Ca_{10}(PO_4)_6F_2$	22.6±20.9**	26.9±8.6*	7.20	0.17
α-TCP	α-$Ca_3(PO_4)_2$	0.0*	7.6±5.1*	6.76	72.62
β-TCP	β-$Ca_3(PO_4)_2$	57.3±6.9	81.1±19.3	7.40	1.27
TTCP	$Ca_4(PO_4)_2O$	78.2±5.0	93.7±6.8	7.65	0.58

*p<0.01 against V79 alone, **p<0.05 against V79 alone, 1)The Ca ions concentration was extracted Ca ions from CP ceramics in PBS(-), which were measured by inductivity coupled plasma-atomic emission spectroscopy.

Table2. Osteogenesis of NHOst cultured on various kinds of CP ceramics.

Samples	Proliferation / %	Differentiation level	
		ALP activity / %	Osteocalcin / %
NHOst alone	100±7.9	100±4.4	100±46.2
HAp	63.2±3.5	20.4±1.8*	81.1±31.0
FAp	42.9±19.5	1.24±0.3*	47.2±20.7
α-TCP	18.3*±2.5	17.9±3.8*	110.7±18.8
β-TCP	56.0±4.7	6.3±3.2*	177.1±78.4**
TTCP	82.3±27.3	17.5±4.6*	114.8±4.0

*p<0.01 against NHOst alone, **p<0.01 against HAp

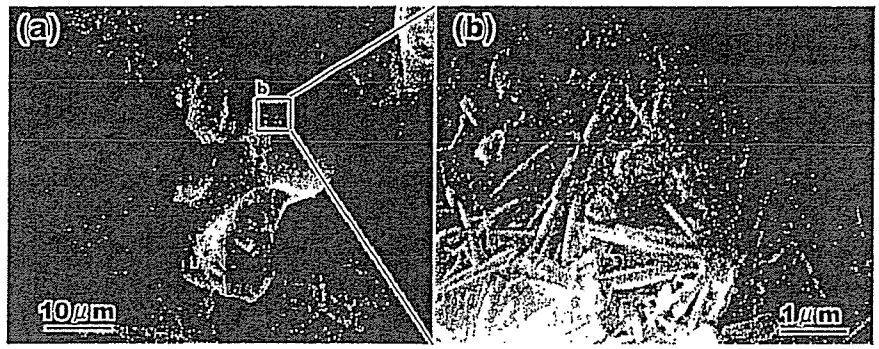

Fig.1. SEM images of α-TCP after extract treatment. (a) whole image and (b) enlarged image of the area enclosed by a rectangle in (a)

Before the extraction, a particle size of α-TCP was about 10μm and its surface was smooth. However, as shown in Fig.1, whisker-like precipitates of 1-2μm in length and 2-300nm in width are observed at the surface of α-TCP after the extraction, although there is no change in its particle size. It is well known that slightly water-soluble calcium phosphates convert to HAp in aqueous solution with high pH value. Since the solubility of α-TCP is higher than that of other calcium phosphates, the α-TCP converts to HAp rapidly as following the reaction.

$$10Ca_3(PO_4)_2+6H_2O \rightarrow 3Ca_{10}(PO_4)_6(OH)_2+2H_3PO_4$$

According to the report of this conversion [4], HAp produced by the above reaction has whisker-like morphology. Therefore, the whisker-like precipitates can be regarded as HAp, so that it is considered that the above conversion occurs at the surface of the α-TCP during incubation. In this case, phosphoric acid is produced as a byproduct in the conversion reaction and the phosphoric acid caused the decrease in the pH of solution. Morita and co-workers [5] have reported that low pH itself could be clastogenic to mammalian cells and the pH of 50% V79 cell survival was 6.5 for 24h incubation. Therefore, it is suggested that the cytotoxicity of α-TCP was mainly due to the pH decreasing resulting from an increase of the phosphoric acid ion produced by the hydrolysis conversion from α-TCP to HAp.

On the other hand, FAp has the same crystal structure of HAp but the hydroxyl ions in HAp substituted by fluorine ions. Since difference of the colony formation on various CP ceramics would be due to eluted substances from CP as described above, the cytotoxicity of FAp would be due to eluted fluoride ions from FAp.

Effects of CP ceramics on osteogenesis function of NHOst are shown in table2. As shown in the table, ALP activities of NHOst were significantly suppressed on CP ceramics irrespective of their type and the amount of osteocalcin on β-TCP was the highest among five kinds of CP ceramics. Since it is well known that osteocalcin express in maturated stage of differentiation level of NHOst, these results suggest that maturation of NHOst proceeds on β-TCP. . The differences of maturation of NHOst on various kinds of CP ceramics may be related with the amount of extracted Ca^{2+} and/or PO_4^{3-} ions.

References

[1] Y. Ito, N. Tanaka, Y. Fujimoto, Y. Yasunaga, O. Ishida, M. Agung, M. and Ochi, J. Biomed. Mater. Res: Vol.69A(3) (2004) p454

[2] K. Cheng K, W. Weng, H. Qu, P. Du, G. Shen, G. Han, J. Yang and M. J. Ferreira: J.Biomed. Mater. Res. B, Vol.69(1) (2004) p33

[3] M. E. Ooms, J. G. C. Wolke, J. C. P. M. Waerden and J. A. Jansen, Trabecular, J.Biomed. Mater. Res. Vol.61 (2002) p9

[4] M.Tamai, T.Isshiki, K.Nishio, M.Nakamura, A.Nakahira and H.Endoh: J. Mater. Res. Vol.18 (2003), p.2633

[5] T.Morita, T.Nagaki, I.Fukuda and K.Okumura: Muta. Res. Vol.268 (1992), p.297

一般報文

ラット頭蓋冠由来骨芽細胞のALPase活性を促進する硫酸化ヒアルロン酸の効果

信州大学繊維学部　石黒（長幡）操・寺本　彰・阿部康次
国立医薬品食品衛生研究所療品部　中岡竜介・土屋利江

Enhancement Action of Sulfated Hyaluronan on the ALPase Activity of Rat Calvarial Osteoblasts

Misao Nagahata-Ishiguro[*1,2], *Ryusuke Nakaoka*[*2], *Toshie Tsuchiya*[*2], *Akira Teramoto*[*1] *and Koji Abe*[*1]

[*1] Department of Functional Polymer Science, Faculty of Textile Science and Technology, Shinshu University, Ueda 386-8567, Japan
[*2] Division of Medical Devices, National Institute of Health Sciences, Tokyo 158-8501, Japan

Abstract : The purpose of this study was to clarify the effect of hyaluronan (Hya) and sulfated hyaluronan (SHya) on rat calvarial osteoblast (rOB) cells proliferation and differentiation *in vitro*. rOB cells were cultured in the presence of Hya with different molecular weights (0.2, 2, 30, 90, 120 x 10^4) for 10days. Hya did not affect the proliferation of rOB cells. However, SHya suppressed the proliferation of rOB cells. The alkaline phosphatase (ALPase) activity of rOB cells cultured with SHya for 10 days was significantly enhanced in comparison with control (in the absence of polysaccharides) and with Hya. Hya suppressed the ALPase activity of rOB cells. As a result, SHya can control rOB cells proliferation and differentiation. SHya suppressed the rOB cells proliferation in a few culture days and promoted the differentiation. It was suggested that these effects were based on the sulfate groups of SHya. Therefore, it is considered that SHya is useful for the biomedical material, which promotes the differentiation of rOB cells.

(Received 16 June, 2004; Accepted 20 December, 2004)

1. 緒　言

硫酸化多糖であるヘパリン（Heparin; Hep）やヘパラン硫酸（Heparan sulfate; HS）はheparin-binding growth factors（HBGFs）と複合体を形成し，組織が損傷を受けた場合，速やかにHBGFsを放出して，周辺の組織を活性化することが明らかとなっている[1-3]．HBGFsは，骨の修復にも重要な役割を果たしていることが知られ，骨芽細胞の増殖や分化の過程でオートクライン，パラクライン的に骨の形成や吸収を制御する[4-6]．病気やケガなどで骨組織が損傷した場合，修復するために人工骨や人工関節などの人工材料が用いられている．しかし，これらの人工材料は様々な問題があり，近年組織工学的手法を用いた骨再生が期待されている．この手法を用いて骨組織の再生に利用される細胞は，骨組織を形成する骨芽細胞である．骨芽細胞は間葉系由来の細胞で，未分化な間葉系の細胞から骨原性細胞を経て次第に成熟した骨芽細胞へと分化する．骨が大きく欠損した場合，細胞が増殖，分化するための足場が失われるため，仮の足場が必要となる．しかし，足場が優れていても細胞の数が少ないと十分な組織の再生は望めない．そこで、生体材料と増殖因子の組み合わせによる組織再生の方法が，近年多く報告されている[7, 8]．しかし，これらの増殖因子はたんぱく質であり，生体内での寿命が短く，不安定であるため，増殖因子を保持する担体が必要である．グリコサミノグリカンの構成成分であるヒアルロン酸（Hya）は，眼球、関節をはじめとする多くの結合組織に存在し，細胞外マトリックスの構成成分として，組織の創傷治癒や形態発生に重要な働きをしていることが報告されている[9-11]．近

年，Hya のレセプターとして CD44 が発見されて以来，Hya を介した生物学的機能の研究が盛んに行われている[12-14]．Pilloni らは，骨芽細胞の前駆細胞である間葉系細胞を用いて，分子量の異なる Hya の影響を検討しており[15]，Hya は骨芽細胞の石灰化を促進すると報告している．しかし，細胞の増殖性，分化マーカーについての詳細な検討は行っていない．そこで本研究では，骨再生用材料の開発を目的として，生体適合性の高い多糖類を用いて骨組織の再生を試みた．本研究では、ヒアルロン酸と硫酸化多糖の機能を併せ持つ高分子量の硫酸化多糖を作製し，ラット頭蓋冠由来骨芽細胞[rat calvarial osteoblast (rOB cells)]の初期骨分化マーカーである Alkaline phosphatase (ALPase) に対する影響について検討を行った．

2. 実験方法

2.1 材料

SHya は以前に報告した方法にて合成した[16]．使用した硫酸化多糖の硫酸化度 (D.S.；2 糖残基当たり硫酸基の量) を Table 1 に示した．HyaX(X は分子量を示す)の分子量は 0.2, 2, 30, 90, 120 x 10^4のもの使用した．Hya, SHya, コンドロイチン硫酸 typeC (Chs-C), Hep は 0.5 mg/l の濃度になるように培地に溶解し，0.22 μm の孔径を有する filter で滅菌をおこなった．Hya および SHya の構造式を Fig.1 に示した．

Table 1 Characteristics of polysaccharides

Polysaccharides	Number of sulfate groups per two saccharide rings	MW (x10^4)
Hya	0	0.2-120
1.2SHya	1.2	55
2.1SHya	2.1	20
3.4SHya	3.4	5
Chs-C	1	0.5
Hep	2.5	1

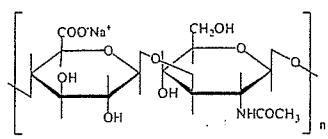

Hyaluronan (Hya)

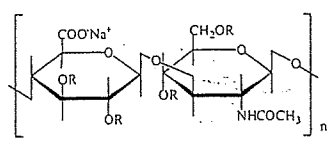

Sulfated hyaluronan (SHya)

R = $SO_3^-Na^+$ or H^+

Fig.1 Structure of hyaluronan and sulfated hyaluronan

2.2 細胞培養

生後 48 時間以内のウィスター系ラット (Charles River) の頭蓋冠から、酵素消化法により rOB cells を分離した[17]．その後，10% fetal bovine serum (FBS, GIBCO) を含む Dulbecco's modified Eagle's medium(DMEM, Nissui-seiyaku) を用いて，初代培養を行った．3 日毎に培地を交換しながら通常の継代培養を行い，継代数 4-6 の rOB cells を実験に使用した．

2.3 細胞増殖

多糖類と 10% FBS を含む DMEM を用いて調製した rOB cells ($1x10^4$ cells/well, 24 multiwell plate) を播種し，5% CO_2 下，37℃で培養した．所定時間培養後の細胞数を，下記のタンパク質量測定によって計測した．上澄みを除去し，well を phosphate-buffered salines (PBS; pH7.6) で 3 回洗浄した。0.04% nonidet P-40 (NP-40, Nacalai tesque) を含む 1ml PBS を各 well に添加し，37℃で 10 分間インキュベートした．懸濁液を超音波破砕機を用いてホモジナイズした後，1000rpm, 4℃, 5 分間遠心を行った．この上澄液を細胞溶液として，Bio-Rad protein assay (protein assay, Bio-Rad Lab.) 法により，595nm の吸光度を EIA READER を使って総タンパク質量を測定した．細胞数とタンパク質量の検量線を作成し，検量線により総タンパク質量から細胞数を算出した．検量線の作成法を以下に示す．0, 1, 5, 10, $30x10^5$ cells/ml に調製した細胞懸濁液を各試験管に入れ，1000rpm, 4℃, 5 分間遠心を行った．上澄みを除去し，0.04% NP-40 を含む 1ml PBS を各試験管に入れ，総タンパク質量を求め，細胞数と総タンパク質量の検量線を作成した．

2.4 Alkaline phosphatase (ALPase) 活性

ALPase 活性の測定は以下のようにして行った．細胞増殖の測定時に得られた細胞溶解液 0.1ml と基質水溶液 0.4ml (16mM p-nitrophenylphosphate disodium salt hexahydrate) を混合して，30 分間，37℃でインキュベートした．その後，反応を停止するため，混合液に 0.2N NaOH 水溶液を 0.5ml 添加し，410nm の吸光度を EIA READER を用いて測定した．総タンパク量は Bio-Rad protein assay によって測定し，Albumin(Bovine Albumin Fraction V) の検量線から算出した．

全ての実験において，実験数 n=6 として測定を行い，その平均値を求めた。

3. 結 果

分子量の異なる Hya を添加した rOB cells の増殖曲線を，Fig.2 に示した．培養 7 日目までは，Hya の分子量に関係なく rOB cells は増殖し，コンフルエントに達した．しかし，培養 10 日目になると，高分子量の Hya を添加した rOB cells において，わずかに細胞数の増加が示され